

Mechanism and Dynamics of Intramolecular C–H Insertion Reactions of 1-Aza-2-azoniaallene Salts

Xin Hong,^{†,§} Daniel A. Bercovici,^{‡,§} Zhongyue Yang,[†] Nezar Al-Bataineh,[‡] Ramya Srinivasan,[‡] Ram C. Dhakal,[‡] K. N. Houk,^{*,†} and Matthias Brewer^{*,‡}

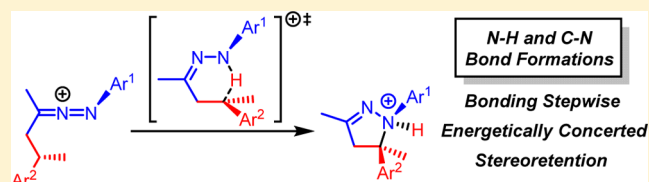
[†]Department of Chemistry and Biochemistry, University of California, Los Angeles, California 90095, United States

[‡]Department of Chemistry, The University of Vermont, Burlington, Vermont 05405, United States

Supporting Information

ABSTRACT: The 1-aza-2-azoniaallene salts, generated from α -chloroazo compounds by treatment with halophilic Lewis acids, undergo intramolecular C–H amination reactions to form pyrazolines in good to excellent yields. This intramolecular amination occurs readily at both benzylic and tertiary aliphatic positions and proceeds at an enantioenriched chiral center with retention of stereochemistry. Competition

experiments show that insertion occurs more readily at an electron-rich benzylic position than it does at an electron-deficient one. The C–H amination reaction occurs only with certain tethers connecting the heteroallene cation and the pendant aryl groups. With a longer tether or when the reaction is intermolecular, electrophilic aromatic substitution occurs instead of C–H amination. The mechanism and origins of stereospecificity and chemoselectivity were explored with density functional theory (B3LYP and M06-2X). The 1-aza-2-azoniaallene cation undergoes C–H amination through a hydride transfer transition state to form the N–H bond, and the subsequent C–N bond formation occurs spontaneously to generate the heterocyclic product. This concerted two-stage mechanism was shown by IRC and quasi-classical molecular dynamics trajectory studies.



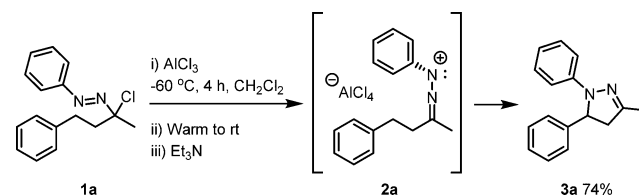
INTRODUCTION

C–H insertions of nitrogen-centered radicals,¹ nitrenes,² and, most notably, transition metal nitrenoids³ are valuable synthetic reactions. On the basis of Breslow and Gellman's seminal work,⁴ Che,⁵ Du Bois,⁶ Driver,⁷ Davies,⁸ Lebel,⁹ and Shi¹⁰ have made C–H insertions of transition metal nitrenoids practical and stereoselective processes for natural product synthesis. Mechanistic studies indicate that both concerted and stepwise radical rebound processes can be operative in these transformations.¹¹

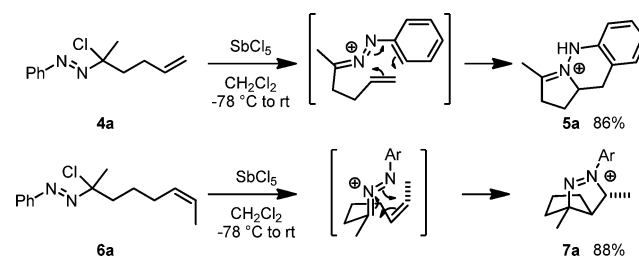
The Brewer group has studied the reactivities of aryl 1-aza-2-azoniaallene salts in intramolecular reactions leading to nitrogen heterocycles.¹² These heteroallene species can be prepared directly from N-aryl hydrazones by oxidation or through the reaction of α -chloroazo compounds with halophilic Lewis acids. As shown in Scheme 1, these species, which can also be considered to be imino-nitrenium cations, undergo direct insertion into pendant benzylic C–H bonds to afford pyrazolines.^{12d}

These 1-aza-2-azoniaallene salts are also known to react with pendant alkenes in (3 + 2) or [4 + 2] cycloadditions to provide various heterocycles, as shown in Scheme 2.^{12a–c,e} The chemo- and regioselectivity of the cycloaddition reactions were found to be controlled by the length of the tether that connects the reacting components. We recently studied these cycloaddition reactions computationally to understand the origins of these substrate-dependent reactivities.¹³ We have now studied the scope of the insertion reaction experimentally and established

Scheme 1. Intramolecular Benzylic C–H Insertion of a 1-Aza-2-azoniaallene



Scheme 2. Intramolecular Cycloadditions of 1-Aza-2-azoniaallenes



the mechanism and determined the origins of selectivities in the insertion process through computation.

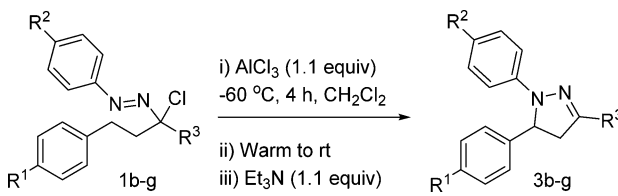
Received: April 29, 2015

Published: July 7, 2015

RESULTS AND DISCUSSION

Experimental Results. Our initial report of the C–H insertion reactivity of aryl 1-aza-2-azoniaallene salts (Table 1)

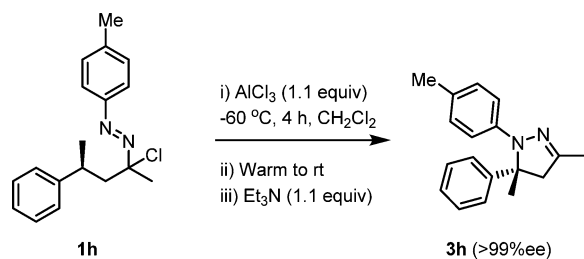
Table 1. Intramolecular C–H Insertions of 1-Aza-2-azoniaallenes with Electron-Rich and -Poor N-Aryl Substituents



entry	α -chloroazo	R ¹	R ²	R ³	yield
1	1b	H	Cl	CH ₃	61%
2	1c	H	CH ₃	CH ₃	79%
3	1d	OCH ₃	Cl	CH ₃	79%
4	1e	CH ₃	Cl	CH ₃	65%
5	1f	NO ₂	Cl	CH ₃	65%
6	1g	OCH ₃	CH ₃	-(CH ₂) ₂ -(4-NO ₂)Ph	92%

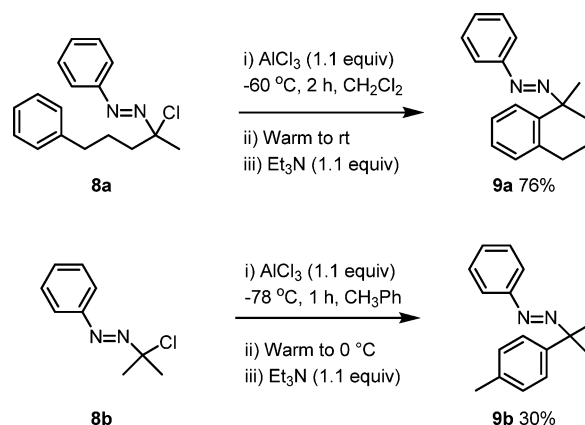
indicated that heteroallenes with electron-rich N-aryl groups provided higher yields of insertion products than those with electron-poor N-aryl groups (entry 1 vs 2, Table 1).^{12d} The electronic properties of the pendant aryl group also affected the C–H insertion (entries 3–6, Table 1). Electron-rich methoxy derivatives gave notably higher yields of insertion, but there was little difference in yield between substrates with neutral and electron-deficient aryl rings (entries 4 and 5). A competition experiment showed that the insertion occurred more readily adjacent to an electron-rich aryl ring than it did adjacent to an electron-deficient one (entry 6). No insertion was observed at a secondary aliphatic center, but insertion did occur at a tertiary aliphatic center. The reaction in Scheme 3 showed that insertion at a chiral tertiary benzylic position occurs with retention of stereochemical purity.

Scheme 3. Stereospecific C–H Insertion of a 1-Aza-2-azoniaallene at a Tertiary Benzylic Position



We have now obtained further experimental data that define the scope and mechanism of this insertion reaction. We explored the effect of tether length on intramolecular C–H insertions. α -Chloroazo **8a** was treated with Lewis acid, AlCl₃, to generate the corresponding 1-aza-2-azoniaallene salt. This heteroallene, which has a tether that is one methylene unit longer than the tether in **1a**, does not undergo the C–H insertion but instead reacts with the pendant aryl group in an electrophilic aromatic substitution reaction to give azotetralin **9a** in 76% yield (Scheme 4). This reactivity highlights the electrophilic nature of heteroallene salts and shows that tether

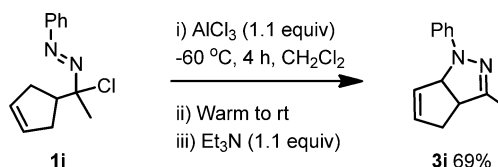
Scheme 4. Effect of Tether Length on Intramolecular Reactions of 1-Aza-2-azoniaallenes



length plays an important role in determining the result of these reactions. This Friedel–Crafts-type reactivity is not limited to intramolecular reactions; the heteroallene derived from acetone reacted with toluene to give azo-cymene **9b** in 30% yield (Scheme 4).

Unlike the well-established allylic C–H aminations with transition metal catalysts, the linear 1-aza-2-azoniaallene salts, such as **4a** and **6a**, undergo [4 + 2] or 1,3-monopolar¹⁴ cycloadditions with pendant alkenes (Scheme 2). In order to achieve allylic C–H amination, we prepared a heteroallene salt of cyclopentene derivative **1i**, which would undergo [4 + 2] cycloaddition only with difficulty due to conformational constraints. Indeed, this substrate underwent allylic insertion instead of cycloaddition to give pyrazoline **3i** in 69% yield (Scheme 5).

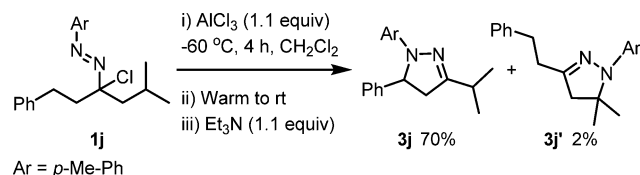
Scheme 5. Intramolecular C–H Insertion of a 1-Aza-2-azoniaallene at an Allylic Position



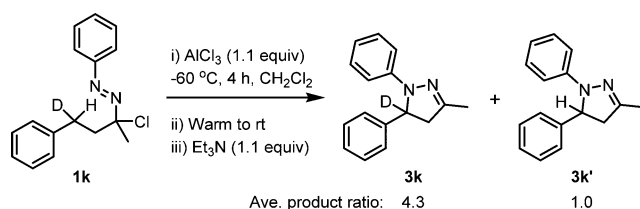
We also studied competition between C–H insertion at benzylic and tertiary aliphatic positions. As a point of comparison, previous studies show that rhodium nitrenoids insert more readily at tertiary aliphatic centers than at benzylic positions,¹⁵ whereas ruthenium^{6h} and iron¹⁶ based catalysts select for benzylic or allylic positions, and the selectivity of silver catalysts is ligand-dependent.¹⁷ To assess the chemoselectivity of 1-aza-2-azoniaallene salt insertions, we prepared the heteroallene salt derived from 5-methyl-1-phenylhexan-3-one (**1j**); insertion occurred almost exclusively at the benzylic position (Scheme 6).

We also conducted a kinetic isotope effect (KIE) study using an internal competition experiment. The requisite deuterium-enriched ketone precursor of α -chloroazo **1k** was prepared by the conjugate reduction procedure described by Keinan and Greenspoon.¹⁸ Subjecting **1k** to the C–H amination reaction conditions provided an average 4.3:1 ratio of deuterated to nondeuterated insertion products (**3k** and **3k'**), as determined by ¹H NMR integration of duplicate experiments (Scheme 7). Changing the N-aryl ring to *p*-tolyl had no effect on the

Scheme 6. Competition between Intramolecular C–H Insertions and Tertiary Aliphatic Positions of 1-Aza-2-azoniaallene



Scheme 7. Experimental Kinetic Isotope Effect



selectivity. KIE studies have been widely applied in mechanistic investigations of other C–H amination reactions. Typically, aminations that occur by a radical rebound mechanism have high KIEs (in the range of 6–12),^{5a} since the transition state involves mainly hydrogen atom transfer. By contrast, aminations that proceed through concerted insertion mechanisms show significantly lower KIEs (typically, 1–3).^{15,6h} KIEs between 3 and 6 seem to indicate rapid radical rebound mechanisms^{17,19} or highly asynchronous concerted insertions.^{6h,9c,20,21} The relatively high primary isotope effect of 4.3 suggests the latter mechanism.

Computational Methods. DFT calculations were performed with Gaussian 09.²² Geometry optimizations were carried out with B3LYP functional and the 6-31G(d) basis set. The vibrational frequencies were computed at the same level to check whether each optimized structure is an energy minimum or a transition state and to evaluate its zero-point vibrational energy (ZPVE) and thermal energies at 298 K. Single-point energies were computed with the M06-2X functional²³ and the 6-311+G(d,p) basis set. Solvation energy corrections for dichloromethane were evaluated by a self-consistent reaction field (SCRF) using the SMD²⁴ model under the same level of theory as the single-point energy calculation (M06-2X/6-311+(d,p)).

The reaction mechanism and timing of bond formations were studied by quasi-classical trajectories at 298 K, with B3LYP and the 6-31G* basis set. All dynamics calculations were performed with Prodyn,²⁵ with which the classical equations of motion are integrated with the velocity Verlet algorithm. Energies and derivatives were computed on the fly using Gaussian 09 with a 1 fs integration step size. Trajectories were initialized, from the structure of the transition state TS11, by TS normal mode sampling and were then propagated in both reactants and products directions.²⁶

Computational Results. Reaction Mechanism. We first studied the insertion reaction mechanism for the 1-aza-2-azoniaallene cation 10 (Figure 1). The optimized structures of transition states and the free energy changes on the singlet and triplet pathways are shown in Figure 1. From the singlet species 10, C–H amination can occur through transition state TS11, with a free energy barrier of 20.0 kcal/mol, leading to the protonated heterocyclic product 12.

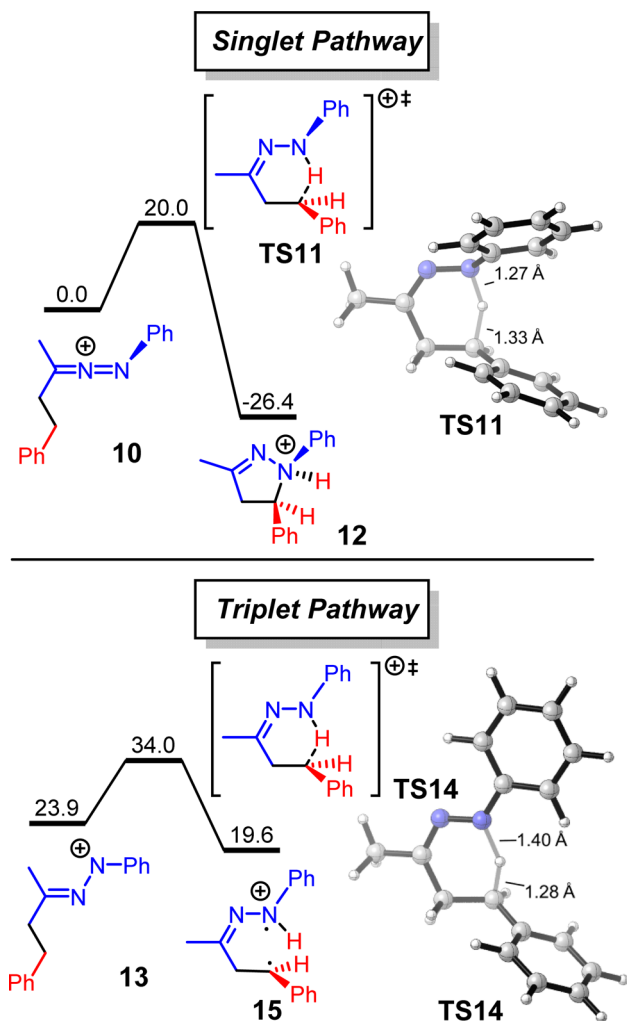


Figure 1. Optimized structures of transition states and free energy changes of singlet and triplet C–H amination pathways of aryl-1-aza-2-azoniaallene 10. Gibbs free energies are in kcal/mol.

Azoniaallene 10 has two moieties that can react: the cationic heterocumulene part and the pendant benzylic C–H bond. In the singlet transition state TS11, the major orbital interaction between the reacting fragments occurs between the LUMO of the 1,3-monopolar heterocumulene fragment and the HOMO of the benzylic C–H bond. This suggests that a hydride abstraction occurs initially to the electron-deficient heterocumulene, forming a N–H bond and a benzyl carbocation. This benzyl carbocation then forms a C–N bond with the remaining lone pair on nitrogen to give the insertion product.

Alternatively, 10 could undergo a spin transition to generate the triplet diradical species, 13, which could react through a triplet C–H amination pathway.²⁷ However, triplet 13 is 23.9 kcal/mol less stable than 10, making the triplet pathway much less favorable as compared with the singlet pathway.

Origins of Stereospecificity of the Singlet C–H Amination Pathway. The bonding stepwise process of the C–H amination seems to be at odds with the stereoselectivity observed for insertion at a chiral benzylic position (Scheme 3). The origin for the stereospecificity is, however, explained by the intrinsic reaction coordinate (IRC) of TS11, shown in Figure 2. Starting from the substrate (point 1), the benzylic hydride gradually moves to the electron-deficient terminal nitrogen via the transition state (point 21) to form the N–H bond (points

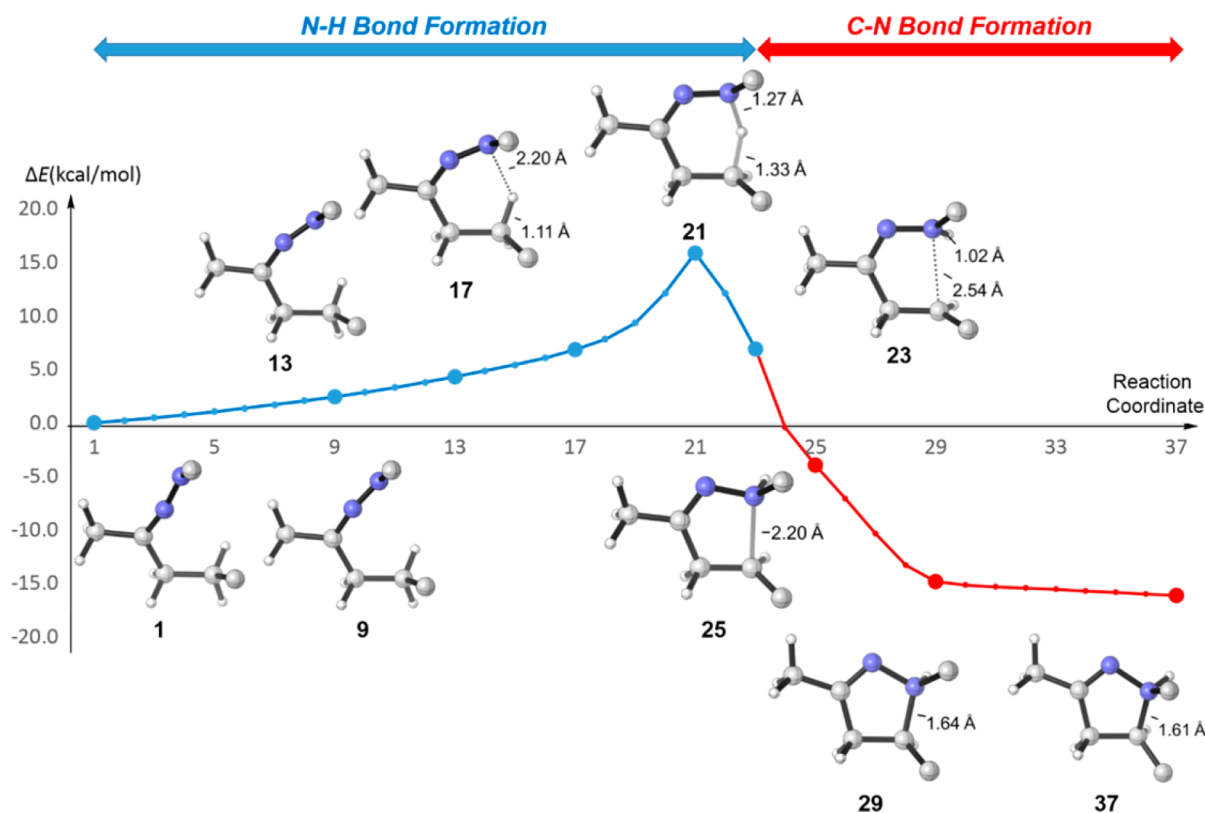


Figure 2. IRC of transition state TS11; only the α -carbons of the phenyl groups are shown for simplicity, and the boundary between N–H and C–N bond formations is chosen based on the N–H bond distance.

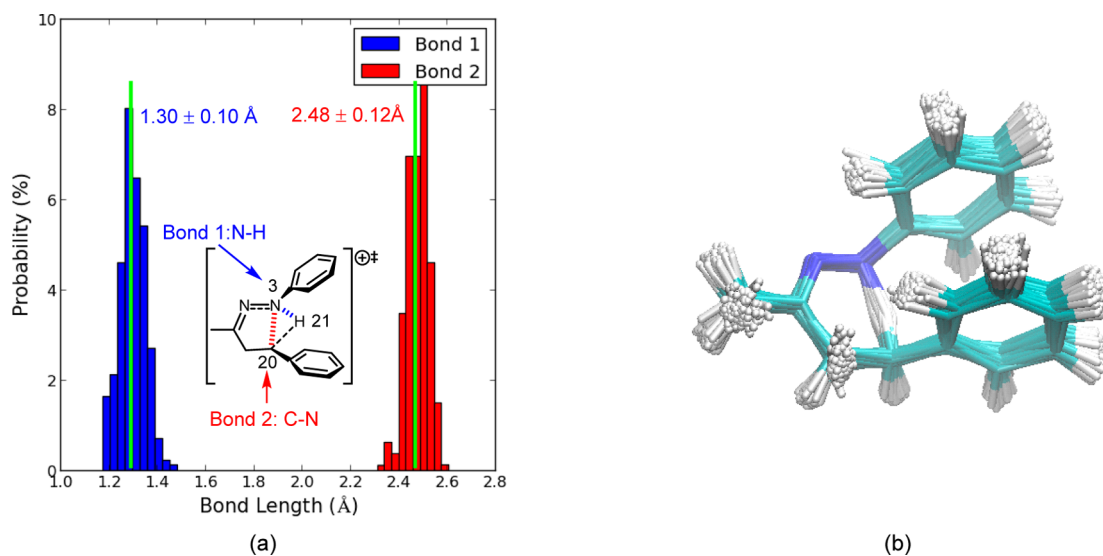


Figure 3. (a) Distribution of N–H and C–N bonding lengths in the transition state region of the singlet C–H amination pathway at 298 K. (b) Superposition of the 256 sampled transition state geometries.

1–23). At point 23, the N–H bond is fully formed with a distance of 1.02 Å, but the C–N distance is still 2.54 Å. The subsequent C–N bond formation then occurs spontaneously, leading to the heterocyclic product (points 23–37). This IRC trajectory indicates that while the singlet C–H amination process is bonding stepwise it is energetically concerted. That is, from substrate to product there is only one saddle point and, after the hydride transfer, there is no stable intermediate; the two consecutive bond formations are energetically concerted and occur via one transition state. This is a nitrogen rebound, in

analogy to the oxygen rebound, which is well-known for cytochrome P-450²⁸ and other related oxidations, like that of dioxirane.²⁹

In order for the insertion to occur at a chiral center without stereomutation, C–N bond formation must occur much faster than C–C bond rotation, which would erode the stereoselectivity, by allowing bond formation with inversion of configuration. To test whether the proposed mechanism accounts for the experimentally observed stereoselectivity, we also studied the insertion pathway through quasi-classical

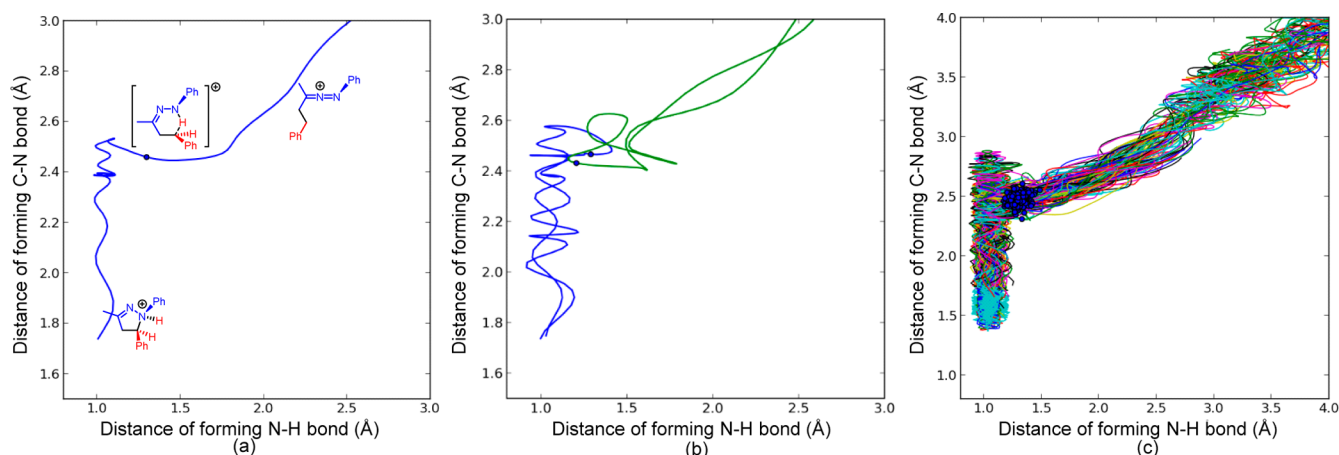


Figure 4. Quasi-classical molecular dynamics trajectories for the singlet C–H amination of aryl-1-aza-2-azoniaallene **10**: (a) A productive trajectory. The duration of the trajectory is 110 fs. (b) Two unproductive trajectories. The green trajectory recrosses at reactant side, and the blue trajectory recrosses at the product side. (c) Overlay of 256 trajectories at 298 K.

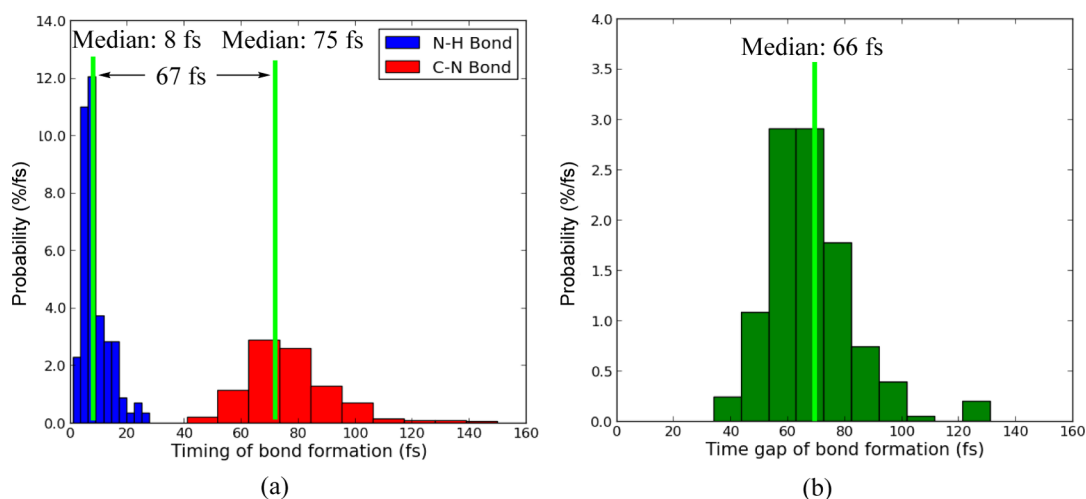


Figure 5. (a) Distribution of timing of C–N and N–H bond formations at 298 K. The starting point (time zero) is each sampled transition state geometry. (b) Distribution of the time gap between C–N and N–H bond formations.

molecular dynamics trajectories to provide information about the timing of bond formations. Quasi-classical trajectories were initialized by transition state normal mode sampling with the Progdyn program developed by Singleton.²⁵ An ensemble of transition states was sampled on the basis of Boltzmann distributions. These form a dividing surface intersecting the saddle point on the potential energy surface. The overlay of sampled transition state geometries and the corresponding C–N and N–H bond length distributions is shown in Figure 3. Both C–N and N–H bond lengths are distributed symmetrically with respect to the bond lengths of the saddle point (marked with green lines in Figure 3). This distribution of bond length is Gaussian, and we define the transition zone as the 98% confidence interval of the Gaussian distribution. The transition zones for the C–N and N–H bonds are 2.48 ± 0.12 and 1.30 ± 0.10 Å, respectively. This means that 98% of the C–N and N–H bond lengths sampled are within ± 0.12 and ± 0.10 Å of the respective bond lengths at the saddle point.

Sampled transition states were propagated forward and backward by Newtonian equations of motion until they reached reactants or products. The fully formed bond length is defined as 1.10 Å for N–H and 1.80 Å for C–N. The corresponding distances in the reactant are 3.00 Å for both bonds. Trajectories

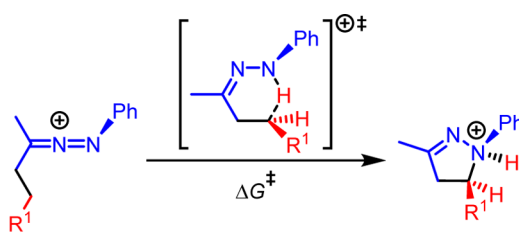
were terminated after 500 fs if they had not reached reactant or product in that period. A total of 256 trajectories was computed, and 95% of these were productive. Figure 4a illustrates one typical productive trajectory: starting from the substrate, the benzylic hydride moves to the terminal nitrogen until the N–H bond is about 1.1 Å, but at this time point, the C–N distance is still around 2.5 Å. The subsequent C–N bond formation occurs spontaneously, accompanied by some residual vibration of the just-formed C–H bond, with the formation of the heterocyclic product. Figure 4b shows two typical unproductive trajectories, which recross in the reactant or product side, and Figure 4c shows the overlay of all 256 trajectories.




Figure 5a shows the distribution of timing of bond formations for all productive trajectories. Starting from the sampled transition state starting geometries, the median time for N–H bond formation (reaching 1.10 Å) is 8 fs, and the median time for C–N bond formation (reaching 1.80 Å) is 75 fs; the timing of C–N bond formation is, on average, 67 fs later than that of N–H bond formation, essentially within a C–N vibrational period. This indicates that the N–H bond forms almost immediately after the transition state saddle point, which is in line with the IRC calculations (Figure 2), and that

the C–N bond forms spontaneously afterward within a short period of time. We also calculated the time gap between the formation of the C–N and N–H bonds for each productive trajectory. The distribution of time gaps is shown in Figure 5b. The time gap of bond formation ranges only from 35 to 130 fs, with the median located at 66 fs. This indicates that there is a short time window between bond formation. Because the time scale of C–C bond rotation is generally longer than 1 ps, there is insufficient time for a C–C bond rotation to occur between the N–H and C–H bond forming events.

Substituent Effect on the Reactivity of C–H Amination. We have also studied the reaction barriers for substrates with a variety of substitutions on the β -phenyl (R^1) or in place of this group; results are shown in Table 2. The α -methylene of R^1 in

Table 2. C–H Amination Barriers of Substituted Aryl 1-Aza-2-azoniaallene Cations^a



entry	R^1	ΔG^\ddagger	entry	R^1	ΔG^\ddagger
1	Ph	20.0	12	OH	15.6
2	H	31.4	13	NH ₂	11.7
3	Me	21.2	14		20.4
4	Et	21.7	15		25.6
5	<i>i</i> Pr	22.8	16		16.3
6	<i>t</i> Bu	22.9	17	<i>o</i> -NO ₂ -Ph	24.0
7	F	27.2	18	<i>m</i> -NO ₂ -Ph	21.3
8	Cl	29.4	19	<i>p</i> -NO ₂ -Ph	22.6
9	CN	33.9	20	<i>o</i> -OMe-Ph	19.2
10	CF ₃	38.6	21	<i>m</i> -OMe-Ph	19.8
11	NO ₂	35.3	22	<i>p</i> -OMe-Ph	17.9

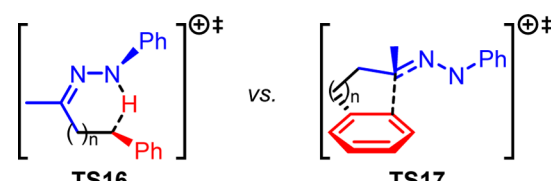
^aGibbs free energies are in kcal/mol.

the substituted 1-aza-2-azoniaallene salt is a hydride donor, and substituents that stabilize the forming carbocation increase the C–H amination reactivities. Replacing the phenyl group (entry 1) by hydrogen (entry 2) increases the barrier dramatically from 20.0 kcal/mol with phenyl to 31.4 kcal/mol with hydrogen. Substitution by alkyl groups (entries 3–6) does not stabilize the forming carbocation as much as the phenyl group, and the reaction barrier increases to 21–23 kcal/mol. The electronic effect has a strong effect on the barrier. The reaction barrier increases significantly with electron-withdrawing substituents (entries 7–11), whereas electron-donating groups reduce the barrier dramatically (entries 12 and 13). Various electron-rich vinyl and aryl substituents have achievable amination barriers (entries 14, 16, and 20–22). The energy

barriers computed for the *p*-NO₂-Ph and *p*-MeO-Ph derivatives (entries 19 and 22) are consistent with the selectivity observed in the competition experiment (Table 1, entry 6). We also computed amination at a tertiary C–H using the 1-aza-2-azoniaallene cation generated from substrate **1j** as a model, and the barrier is 17.2 kcal/mol.³⁰ The additional alkyl substituent lowers the barrier of amination by stabilizing the forming carbon cation in the transition state, making it competitive with benzylic C–H amination.

Tether Effect on the Competition between C–H Amination and Electrophilic Aromatic Substitution. We also explored the tether effect on the competition between the C–H amination and electrophilic aromatic substitution (Table 3). When there is one methylene between the

Table 3. Gibbs Free Energy Barriers of C–H Amination and Electrophilic Aromatic Substitution of Aryl 1-Aza-2-azoniaallene Cations with Different Tethers^a



n	TS16	TS17
1	20.0	21.3
2	23.8	14.2
3	32.5	20.1
intermolecular	34.4	26.5

^aGibbs free energies are in kcal/mol.

heteroallene component and the benzylic hydride donor ($n = 1$), the C–H amination transition state is 1.3 kcal/mol more stable than the electrophilic aromatic substitution transition state because of the proximity of the reacting partners in **TS16** and the strain in **TS17**. This preference is also in line with the experimental results that this tether causes the C–H amination. With longer tethers ($n = 2, 3$), the chemoselectivity is reversed, and the aromatic substitution is significantly more favorable than C–H amination.³¹ A similar preference is also found in intermolecular reactions; the C–H amination between the corresponding 1-aza-2-azoniaallene and toluene has a barrier of 34.4 kcal/mol, whereas the barrier of electrophilic aromatic substitution is only 26.5 kcal/mol. Therefore, the electrophilic aromatic substitution is intrinsically much more favorable than the C–H amination. Only with the short tether ($n = 1$) does the ring strain of the two competing transition states significantly favor the C–H amination, leading to the reversed chemoselectivity.

CONCLUSIONS

The scope, mechanism, and dynamics of C–H amination reactions of 1-aza-2-azoniaallene salts have been studied experimentally and computationally. The facility of this C–H amination relies heavily on the tether that connects the heteroallene cation component and the pendant aryl groups. While the insertion occurs readily at benzylic and tertiary aliphatic positions when the tether is two methylene units, a longer tether or intermolecular reaction gives electrophilic aromatic substitution, the intrinsically favored reaction, rather than C–H amination.

This C–H amination proceeds through a hydride transfer transition state to form a N–H bond initially, and the subsequent C–N bond formation occurs spontaneously afterward to generate the heterocyclic product. IRC trajectory indicates that the two consecutive bond formation processes, N–H and C–N, are energetically concerted, and this concerted mechanism is further proved by quasi-classical molecular dynamics trajectory studies. The C–N bond formation occurs much faster than C–C bond rotation, which explains the stereospecificity in the C–H amination. In line with the hydride transfer transition state, electron-rich aryl substituents that stabilize the forming carbon cation facilitate the amination significantly, whereas alkyl and electron-poor aryl-substituted substrates have higher reaction barriers.

■ ASSOCIATED CONTENT

● Supporting Information

Experimental procedures and full characterization of the products and spectra. Coordinates, absolute electronic energies, and free energies in solution of DFT-computed stationary points. The Supporting Information is available free of charge on the ACS Publications website at DOI: 10.1021/jacs.5b04474.

■ AUTHOR INFORMATION

Corresponding Authors

*(K.N.H.) houk@chem.ucla.edu

*(M.B.) matthias.brewer@uvm.edu

Author Contributions

[§]X.H. and D.B. contributed equally to this work.

Notes

The authors declare no competing financial interest.

■ ACKNOWLEDGMENTS

We are grateful to the National Scientific Foundation (CHE-1361104 to K.N.H. and CHE-1362286 to M.B.) for financial support of this research. Calculations were performed on the Hoffman2 Cluster at UCLA and the Extreme Science and Engineering Discovery Environment (XSEDE), which is supported by the NSF (OCI-1053575). Mass spectrometry data was acquired by Bruce O'Rourke on instruments purchased through instrumentation grants provided by the NSF (CHE-0821501) and the NIH (S10 OD018126).

■ REFERENCES

- (1) For selected reviews, see: (a) Danen, W. C.; Neugebauer, F. A. *Angew. Chem., Int. Ed. Engl.* **1975**, *14*, 783. (b) Stella, L. *Angew. Chem., Int. Ed. Engl.* **1983**, *22*, 337. (c) Zard, S. Z. *Chem. Soc. Rev.* **2008**, *37*, 1603. For recent examples, see: (d) Cecere, G.; König, C. M.; Alleva, J. L.; MacMillan, D. W. C. *J. Am. Chem. Soc.* **2013**, *135*, 11521. (e) Allen, L. J.; Cabrera, P. J.; Lee, M.; Sanford, M. S. *J. Am. Chem. Soc.* **2014**, *136*, 5607. (f) Foo, K.; Sella, E.; Thomé, I.; Eastgate, M. D.; Baran, P. S. *J. Am. Chem. Soc.* **2014**, *136*, 5279. (g) Kim, H.; Kim, T.; Lee, D. G.; Roh, S. W.; Lee, C. *Chem. Commun.* **2014**, *50*, 9273. (h) Qin, Q.; Yu, S. *Org. Lett.* **2014**, *16*, 3504. (i) Greulich, T. W.; Daniliuc, C. G.; Studer, A. *Org. Lett.* **2015**, *17*, 254. (j) Louillat-Habermeyer, M.-L.; Jin, R.; Patureau, F. W. *Angew. Chem., Int. Ed.* **2015**, *54*, 4102.
- (2) For selected reviews, see: (a) Collet, F.; Lescot, C.; Liang, C.; Dauban, P. *Dalton Trans.* **2010**, *39*, 10401. (b) Dequirez, G.; Pons, V.; Dauban, P. *Angew. Chem., Int. Ed.* **2012**, *51*, 7384.
- (3) For selected reviews, see: (a) Che, C.-M.; Lo, V. K.-Y.; Zhou, C.-Y.; Huang, J.-S. *Chem. Soc. Rev.* **2011**, *40*, 1950. (b) Davies, H. M. L.;

Lian, Y. *Acc. Chem. Res.* **2012**, *45*, 923. (c) Yamaguchi, J.; Yamaguchi, A. D.; Itami, K. *Angew. Chem., Int. Ed.* **2012**, *51*, 8960.

(4) (a) Breslow, R.; Gellman, S. L. *J. Chem. Soc., Chem. Commun.* **1982**, 1400. (b) Breslow, R.; Gellman, S. L. *J. Am. Chem. Soc.* **1983**, *105*, 6728.

(5) (a) Au, S.-M.; Huang, J.-S.; Yu, W.-Y.; Fung, W.-H.; Che, C.-M. *J. Am. Chem. Soc.* **1999**, *121*, 9120. (b) Yu, X.-Q.; Huang, J.-S.; Zhou, X.-G.; Che, C.-M. *Org. Lett.* **2000**, *2*, 2233. (c) Liang, J.-L.; Yuan, S.-X.; Huang, J.-L.; Yu, W.-Y.; Che, C.-M. *Angew. Chem., Int. Ed.* **2002**, *41*, 3465. (d) Leung, S. K.-Y.; Tsui, W.-M.; Huang, J.-S.; Che, C.-M.; Liang, J.-L.; Zhu, N. *J. Am. Chem. Soc.* **2005**, *127*, 16629. (e) Thu, H. Y.; Yu, W. Y.; Che, C.-M. *J. Am. Chem. Soc.* **2006**, *128*, 9048. (f) Lin, X.; Zhao, C.; Che, C.-M.; Ke, Z.; Phillips, D. L. *Chem. - Asian J.* **2007**, *2*, 1101. (g) Liu, Y.; Guan, X.; Wong, E. L.-M.; Liu, P.; Huang, J.-S.; Che, C.-M. *J. Am. Chem. Soc.* **2013**, *135*, 7194. (h) Wei, J.; Xiao, W.; Zhou, C.-Y.; Che, C.-M. *Chem. Commun.* **2014**, *50*, 3373. (i) Liu, Y.; Chen, G.-Q.; Tse, C.-W.; Guan, X.; Xu, Z.-J.; Huang, J.-S.; Che, C.-M. *Chem. - Asian J.* **2015**, *10*, 100.

(6) (a) Espino, C. G.; Du Bois, J. *Angew. Chem., Int. Ed.* **2001**, *40*, 598. (b) Hinman, A.; Du Bois, J. *J. Am. Chem. Soc.* **2003**, *125*, 11510. (c) Espino, C. G.; Fiori, K. W.; Kim, M.; DuBois, J. *J. Am. Chem. Soc.* **2004**, *126*, 15378. (d) Fleming, J. J.; Du Bois, J. *J. Am. Chem. Soc.* **2006**, *128*, 3926. (e) Kurokawa, T.; Mihyong, K.; Du Bois, J. *Angew. Chem., Int. Ed.* **2009**, *48*, 2777. (f) Du Bois, J. *Org. Process Res. Dev.* **2011**, *15*, 758. (g) Olson, D. E.; Maruniak, A.; Malhotra, S.; Trost, B. M.; Du Bois, J. *Org. Lett.* **2011**, *13*, 3336. (h) Harvey, M. E.; Musaev, D. G.; Du Bois, J. *J. Am. Chem. Soc.* **2011**, *133*, 17207. (i) Roizen, J. L.; Harvey, M. E.; Du Bois, J. *Acc. Chem. Res.* **2012**, *45*, 911. (j) Olson, D. E.; Roberts, D. A.; Du Bois, J. *Org. Lett.* **2012**, *14*, 6174. (k) Roizen, J. L.; Zalatan, D. N.; Du Bois, J. *Angew. Chem., Int. Ed.* **2013**, *52*, 11343. (l) Bess, E. N.; Deluca, R. J.; Tindall, D. J.; Oderinde, M. S.; Roizen, J. L.; Du Bois, J.; Sigman, M. S. *J. Am. Chem. Soc.* **2014**, *136*, 5783. (m) Olson, D. E.; Su, J. Y.; Roberts, D. A.; Du Bois, J. *J. Am. Chem. Soc.* **2014**, *136*, 13506.

(7) (a) Stokes, B. J.; Dong, H.; Leslie, B. E.; Pumphrey, A. L.; Driver, T. G. *J. Am. Chem. Soc.* **2007**, *129*, 7500. (b) Shen, M.; Leslie, B. E.; Driver, T. G. *Angew. Chem., Int. Ed.* **2008**, *47*, 5056. (c) Sun, K.; Sachwani, R.; Richert, K. J.; Driver, T. G. *Org. Lett.* **2009**, *11*, 3598. (d) Nguyen, Q.; Sun, K.; Driver, T. G. *J. Am. Chem. Soc.* **2012**, *134*, 7262. (e) Nguyen, Q.; Nguyen, T.; Driver, T. G. *J. Am. Chem. Soc.* **2013**, *135*, 620. (f) Kong, C.; Jana, N.; Driver, T. G. *Org. Lett.* **2013**, *15*, 824.

(8) (a) Reddy, R. P.; Davies, H. M. L. *Org. Lett.* **2006**, *8*, 5013. (b) Davies, H. M. L.; Manning, J. R. *Nature* **2008**, *451*, 417. (c) Alford, J.; Davies, H. M. L. *J. Am. Chem. Soc.* **2014**, *136*, 10266.

(9) (a) Lebel, H.; Huard, K.; Lectard, S. *J. Am. Chem. Soc.* **2005**, *127*, 14198. (b) Lebel, H.; Huard, K. *Org. Lett.* **2007**, *9*, 639. (c) Huard, K.; Lebel, H. *Chem. - Eur. J.* **2008**, *14*, 6222. (d) Lebel, H.; Spitz, C.; Leogane, O.; Trudel, C.; Parmentier, M. *Org. Lett.* **2011**, *13*, 5460. (e) Lebel, H.; Trudel, C.; Spitz, C. *Chem. Commun.* **2012**, *48*, 7799. (f) Lebel, H.; Piras, H.; Bartholoméüs, J. *Angew. Chem., Int. Ed.* **2014**, *53*, 7300.

(10) Yang, M.; Su, B.; Wang, Y.; Chen, K.; Jiang, X.; Zhang, Y.-F.; Zhang, X.-S.; Chen, G.; Cheng, Y.; Cao, Z.; Guo, Q.-Y.; Wang, L.; Shi, Z.-J. *Nat. Commun.* **2014**, *5*, 4707.

(11) Perry, R. H.; Cahill, T. J.; Roizen, J. L.; Du Bois, J.; Zare, R. N. *Proc. Natl. Acad. Sci. U. S. A.* **2012**, *109*, 18295.

(12) (a) Javed, M. I.; Wyman, J. M.; Brewer, M. *Org. Lett.* **2009**, *11*, 2189. (b) Wyman, J.; Javed, M. I.; Al-Bataineh, N.; Brewer, M. *J. Org. Chem.* **2010**, *75*, 8078. (c) Al-Bataineh, N. Q.; Brewer, M. *Tetrahedron Lett.* **2012**, *53*, 5411. (d) Bercovici, D. A.; Brewer, M. *J. Am. Chem. Soc.* **2012**, *134*, 9890. (e) Bercovici, D. A.; Ogilvie, J. M.; Tsvetkov, N.; Brewer, M. *Angew. Chem., Int. Ed.* **2013**, *52*, 13338.

(13) Hong, X.; Liang, Y.; Brewer, M.; Houk, K. N. *Org. Lett.* **2014**, *16*, 4260.

(14) Hong, X.; Küçük, H. B.; Maji, M. S.; Yang, Y.-F.; Rueping, M.; Houk, K. N. *J. Am. Chem. Soc.* **2014**, *136*, 13769 and references therein.

(15) Fiori, K. W.; Espino, C. G.; Brodsky, B. H.; Du Bois, J. *Tetrahedron* **2009**, *65*, 3042.

(16) Paradine, S. M.; White, M. C. *J. Am. Chem. Soc.* **2012**, *134*, 2036.

(17) Alderson, J. M.; Phelps, A. M.; Scamp, R. J.; Dolan, N. S.; Schomaker, J. M. *J. Am. Chem. Soc.* **2014**, *136*, 16720.

(18) Keinan, E.; Greenspoon, N. *J. Am. Chem. Soc.* **1986**, *108*, 7314.

(19) Badiei, Y. M.; Dinescu, A.; Dai, X.; Palomino, R. M.; Heinemann, F. W.; Cundari, T. R.; Warren, T. H. *Angew. Chem., Int. Ed.* **2008**, *47*, 9961.

(20) Nägeli, I.; Baud, C.; Bernardinelli, G.; Jacquier, Y.; Moraon, M.; Müllet, P. *Helv. Chim. Acta* **1997**, *80*, 1087.

(21) Mueller, P.; Baud, C.; Naegeli, I. *J. Phys. Org. Chem.* **1998**, *11*, 597.

(22) Frisch, M. J.; Trucks, G. W.; Schlegel, H. B.; Scuseria, G. E.; Robb, M. A.; Cheeseman, J. R.; Scalmani, G.; Barone, V.; Mennucci, B.; Petersson, G. A.; Nakatsuji, H.; Caricato, M.; Li, X.; Hratchian, H. P.; Izmaylov, A. F.; Bloino, J.; Zheng, G.; Sonnenberg, J. L.; Hada, M.; Ehara, M.; Toyota, K.; Fukuda, R.; Hasegawa, J.; Ishida, M.; Nakajima, T.; Honda, Y.; Kitao, O.; Nakai, H.; Vreven, T.; Montgomery, J. A., Jr.; Peralta, J. E.; Ogliaro, F.; Bearpark, M.; Heyd, J. J.; Brothers, E.; Kudin, K. N.; Staroverov, V. N.; Kobayashi, R.; Normand, J.; Raghavachari, K.; Rendell, A.; Burant, J. C.; Iyengar, S. S.; Tomasi, J.; Cossi, M.; Rega, N.; Millam, J. M.; Klene, M.; Knox, J. E.; Cross, J. B.; Bakken, V.; Adamo, C.; Jaramillo, J.; Gomperts, R.; Stratmann, R. E.; Yazyev, O.; Austin, A. J.; Cammi, R.; Pomelli, C.; Ochterski, J. W.; Martin, R. L.; Morokuma, K.; Zakrzewski, V. G.; Voth, G. A.; Salvador, P.; Dannenberg, J. J.; Dapprich, S.; Daniels, A. D.; Farkas, O.; Foresman, J. B.; Ortiz, J. V.; Cioslowski, J.; Fox, D. J. *Gaussian 09*, revision D.01; Gaussian, Inc.: Wallingford, CT, 2009.

(23) (a) Zhao, Y.; Truhlar, D. *Theor. Chem. Acc.* **2008**, *120*, 215.

(b) Zhao, Y.; Truhlar, D. G. *Acc. Chem. Res.* **2008**, *41*, 157.

(24) Marenich, A. V.; Cramer, C. J.; Truhlar, D. G. *J. Phys. Chem. B* **2009**, *113*, 6378.

(25) Singleton, D. A.; Hang, C.; Szymanski, M. J.; Greenwald, E. E. *J. Am. Chem. Soc.* **2003**, *125*, 1176.

(26) The criteria to terminate trajectories were as follows: C20–N3 < 1.60 and H21–N3 < 1.10, or C20–H21 < 1.10 and C20–N3 > 5.00 (the atom index is shown in Figure 3). If none of the above criteria were met, then a trajectory was terminated after 500 fs. About 10% of trajectories recross the transition state region to form the same species in the forward and reverse directions, and these trajectories are not discussed.

(27) The possible singlet diradical transition state cannot be located; all optimizations for the corresponding singlet diradical intermediate led to the stable close-shell species **10**. The energy of the singlet species based on the optimized structure of triplet **13** is 29.2 kcal/mol less stable than **10**.

(28) (a) Newcomb, M.; Toy, P. H. *Acc. Chem. Res.* **2000**, *33*, 449.

(b) Groves, J. T. *J. Inorg. Biochem.* **2006**, *100*, 434.

(29) Zou, L.; Paton, R. S.; Eschenmoser, A.; Newhouse, T. R.; Baran, P. S.; Houk, K. N. *J. Org. Chem.* **2013**, *78*, 4037.

(30) The calculated chemoselectivity of substrate **1j** is different than the experimental value (Scheme 6) because the tertiary C–H amination transition state is overstabilized by the solvation energy corrections. In gas phase calculations, benzylic C–H amination is favored by 2.6 kcal/mol. With the CPCM model (Radii = UA0), the chemoselectivity is 1.4 kcal/mol in favor of tertiary C–H amination.

(31) When $n = 3$, the electrophilic aromatic substitution appears to be attainable. However, neither reaction occurred experimentally, and the only identifiable product of this reaction was the corresponding ketone, which presumably forms by hydrolysis during workup.